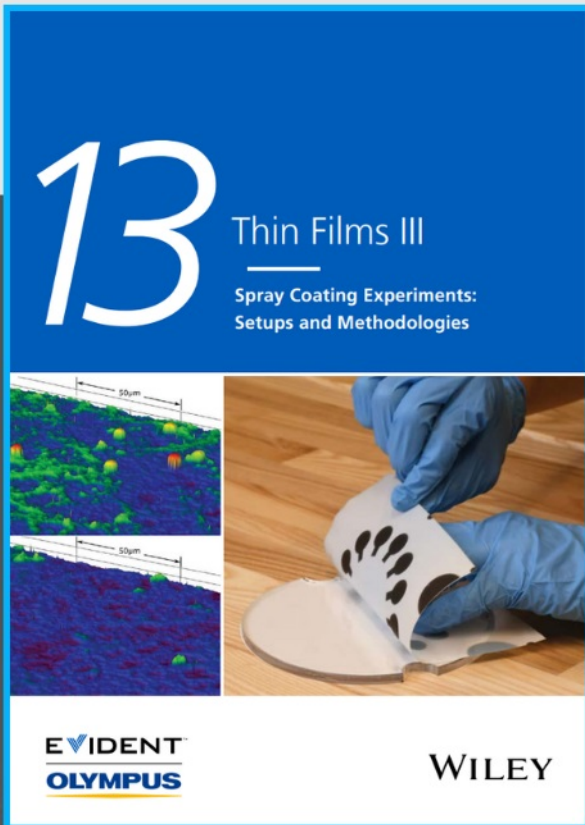




Spray Coating Experiments: Setups and Methodologies



**The latest eBook from
Advanced Optical Metrology.
Download for free.**

Spray Coating Experiments: Setups and Methodologies, is the third in our Thin Films eBook series. This publication provides an introduction to spray coating, three article digests from Wiley Online Library and the latest news about Evident's Image of the Year Award 2022.

Wiley in collaboration with Evident, are committed to bridging the gap between fundamental research and industrial applications in the field of optical metrology. We strive to do this by collecting and organizing existing information, making it more accessible and useful for researchers and practitioners alike.

EVIDENT
OLYMPUS

WILEY

Quinoxaline-Based X-Shaped Sensitizers as Self-Assembled Monolayer for Tin Perovskite Solar cells

Shakil N. Afraj, Chun-Hsiao Kuan, Jian-Sing Lin, Jen-Shyang Ni, Arulmozhi Velusamy, Ming-Chou Chen,* and Eric Wei-Guang Diau*

Four X-shaped quinoxaline-based organic dyes, PQx (1), TQx, (2), PQxD (3), and TQxD (4) (D = dye sensitizers) are developed and served as *p*-type self-assemble monolayer (SAM) for tin perovskite solar cells (TPSC). Thermal, optical, and electrochemical properties of these SAMs are thoroughly investigated and characterized. Tin perovskite layers are successfully deposited on these four SAM surfaces according to a two-step approach and the devices exhibit power conversion efficiency in the order of TQxD (8.3%) > TQx (8.0%) > PQxD (7.1%) > PQx (6.1%). With thiophene π -extended conjugation unit in SAM structure, TQxD (4) exhibits the highest hole extraction rates, greatest hole mobilities, and slowest charge recombination to achieve great device performance of 8.3%, which is the current best result for SAM-based TPSC ever reported. Furthermore, all devices except PQx shows great enduring stability for the performance retaining $\approx 90\%$ of their original values for shelf storage over 1600 h.

1. Introduction

Since solar energy is the largest potential source of carbon-free energy, the development of highly efficient solar cells is envisioned as the efficient way to transform sunlight directly into

electricity.^[1] Among them, perovskite solar cells (PSCs) have attracted much attention due to their rapid performance progress to attain power conversion efficiency (PCE) 25.8% comparable to the Si-based solar cells.^[2–13] However, the toxic lead element in a PSC becomes an issue to be resolved.^[14] Tin PSC (TPSC) thus becomes a potential candidate for the development of lead-free PSC to attain record PCE 14.8% with a 2D/3D device architecture.^[15] Even though the performance of TPSC is far behind its lead analog, the bandgap of a tin perovskite is smaller than a lead perovskite so that TPSC should have a higher theoretical PCE than a lead-based PSC.^[16,17] Many additive engineering strategies were applied to suppress Sn²⁺/Sn⁴⁺ oxidation, passivate the surface defects

and regulate the crystal growth in a TPSC.^[18–24] As reported in the literature, most high-performance TPSC used PEDOT:PSS as hole-transport material (HTM) with deposition of the tin perovskite layer according to a one-step method.^[25–28] This is because the precursor reaction between SnI₂ and FAI (FA represents formamidinium) is very rapid and a hydrophilic HTM like PEDOT:PSS is required for rapid nucleation.^[29] However, PEDOT:PSS is hygroscopic and this would lead to the device performance to be easily degraded in a moisture environment.^[30] To replace hydrophilic PEDOT:PSS by other HTMs with better stability and energy level alignment with tin perovskites, a two-step deposition approach was successfully developed to work with hydrophobic HTM like PTAA.^[31–34]

Recently, PEDOT:PSS was replaced by small organic molecules forming self-assemble monolayer (SAM) on ITO surface for TPSC.^[35] Using SAM to replace PEDOT:PSS for TPSC has several advantages.^[36–38] First, SAM is composed of small organic molecules that can be easily synthesized via chemical methods.^[39,40] Second, SAM forms a very thin and compact layer between tin perovskite and ITO that it helps on hole transfer from perovskite to ITO via SAM and prevents back charge recombination to occur.^[41,42] Third, to match the energy level with tin perovskite, the SAM molecules are easy to modify by changing varied functional groups of the molecule.^[43] To date, several π -conjugated organic molecules as SAMs have been explored for lead-based PSCs.^[44] For instance, Palomares et al. successfully replaced the most common *p*-type HTL, PEDOT:PSS, in the *p*-i-n PSC with a SAMs; PTA, MC-43,^[43] EADR03, and EADR04,^[38] on ITO which led to a considerable

S. N. Afraj, A. Velusamy, M.-C. Chen


Department of Chemistry
and Research Center of New Generation Light Driven Photovoltaic,
Modules

National Central University
Taoyuan 32001, Taiwan
E-mail: mcchen@ncu.edu.tw

C.-H. Kuan, J.-S. Lin, E. W.-G. Diau
Department of Applied Chemistry and Institute of Molecular Science
National Yang Ming Chiao Tung University
1001 Ta-Hseuh Rd., Hsinchu 300093, Taiwan
E-mail: diau@nycu.edu.tw

C.-H. Kuan, J.-S. Lin, E. W.-G. Diau
Center for Emergent Functional Matter Science
National Yang Ming Chiao Tung University
1001 Ta-Hseuh Rd., Hsinchu 300093, Taiwan

J.-S. Ni
Department of Chemical and Materials Engineering
Photo-sensitive Material Advanced Research and Technology Center
(Photo-SMART)
National Kaohsiung University of Science and Technology
Kaohsiung 80778, Taiwan

 The ORCID identification number(s) for the author(s) of this article can be found under <https://doi.org/10.1002/adfm.202213939>.

DOI: 10.1002/adfm.202213939

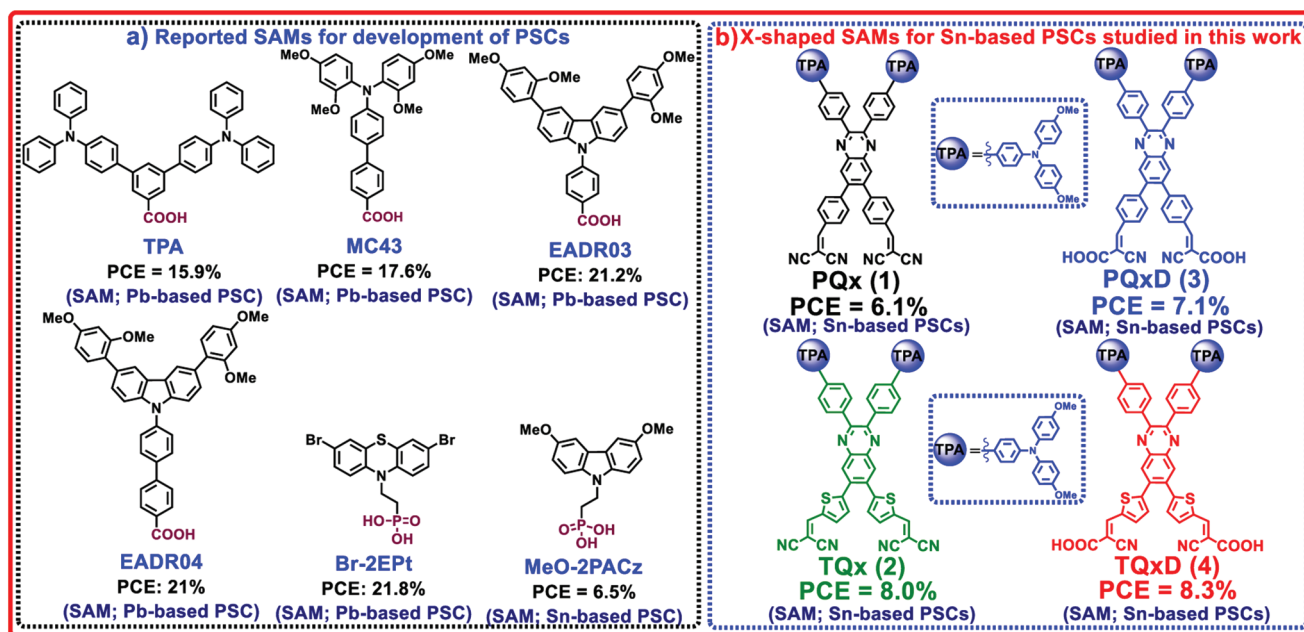


Figure 1. a) Chemical structure of reported self-assembled monolayers (SAMs) for the PSCs. b) Chemical structures of SAMs; PQx (1), TQx (2), PQxD (3) and TQxD (4) for Sn-based PSCs studied in this work.

enhancement in PCE from 17.6% to 21% for Pb-based PSCs. Furthermore, Hong et. al. reported phenothiazine based, SAM; Br-2EPT exhibiting a PCE of 22.44% for Pb-based PSCs.^[42] Despite the impressive progress in the development of SAMs for Pb-based PSCs, there is a significant interest in designing new SAMs for less toxic tin PSCs. Therefore our group recently introduced promising SAM; MeO-2PACz^[35] exhibiting PCE of 6.5% for tin PSCs (**Figure 1a**).

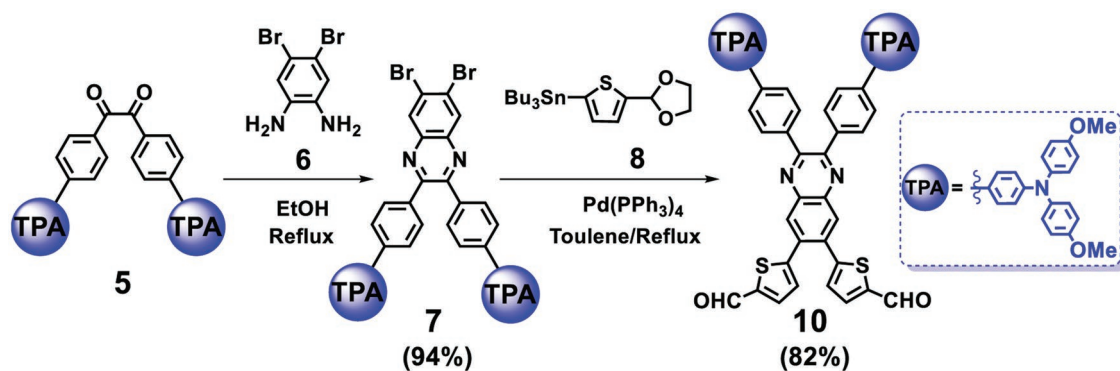
Quinoxaline is a moderately electron-withdrawing molecule and it can be modified to stabilize the HOMO energy level for matching with the valence band (VB) level of perovskite, maintain a high LUMO energy level for blocking electrons from the conduction band (CB) level of perovskite, with great intrinsic photo and thermal stabilities to be applied for TPSC.

Furthermore, regarding design of organic molecules for PSCs, research on dye-sensitized solar cells (DSSCs) where many of metal-free dyes have been developed could give a hint.^[45] In DSSCs, a functional anchoring group (cyanoacrylic acid) is an essential for molecular design, which anchors dyes on a semiconducting TiO₂ nanocrystal surface and leads to enhanced electron injection from the excited dye to TiO₂. Coincidentally, such anchoring groups (cyanoacrylic acid) can also function as efficient passivation sites for perovskite films owing to their Lewis base characteristic to form a coordination interaction with Pb²⁺ ion defects.^[46] Similar to their chemical interactions with metal oxides, such carboxylic and/or cyano groups can also adsorb onto the surface of an indium tin oxide (ITO) electrode, modify the work function of an ITO electrode, and improve interfacial interactions as confirmed in previous works.^[47] Moreover, these carboxylic and/or cyano-based highly polar functional groups have potential in enabling good solubility of the corresponding compounds in polar solvents, a much-desired property for solution processable device fabrication.^[48]

Inspired by above findings, in the present study, we used the quinoxaline moiety as a core species to build a series of X-shaped SAM molecules.^[49,50] To the best of our knowledge D-A type quinoxaline-based X-shaped SAMs for tin perovskite have never been reported. **Figure 1b** shows the chemical structures of four SAM molecules studied in this work, labeled as PQx (1), TQx (2), PQxD (3), and TQxD (4). The main objective of the work presented herein is to demonstrate the novel X-shaped D-A type organic SAMs (1-4) molecular design for use in TPSC. With two anchoring groups (CN or/and -COOH) presented at both ends of quinoxaline core, the new X-shaped SAM have relatively stronger anchoring capacity to the ITO surface to form better molecular arrangement on the surface.^[51,52] This special X-shaped molecular design will help to direct the photoinduced charge transfer and thus enhance the degree of hole injection to the ITO. Whereas common linear-shaped dyes^[53] with only one anchoring group might not be well aligned on the surface^[54] in comparison to the dyes containing two anchoring groups.^[52] In addition, with the two well aligned electron donating TPA groups at both top of the quinoxaline core, the new X-shaped SAM should possess good interaction with perovskite layer, which should lead to better solar cell efficiency.

2. Results and Discussion

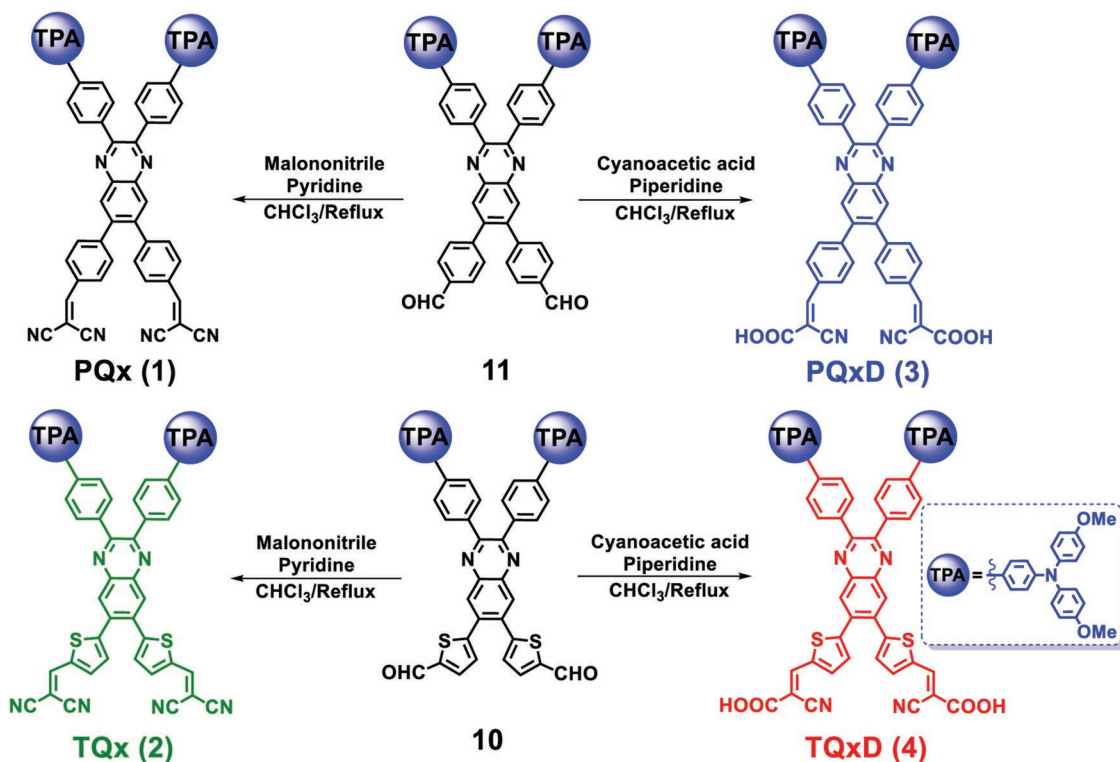
The synthetic routes for SAM molecules 1–4 are shown in **Schemes 1** and **2**, and **Scheme S1** (Supporting Information). Compound **7** was synthesized via coupling of 1,2-bis(4-(bis(4-methoxyphenyl)methyl)-[1,1'-biphenyl]-4-yl)ethane-1,2-dione **5** with 4,5-dibromobenzene-1,2-diamine **6** in refluxing ethanol in an excellent yield (≈94%). Further, intermediates **10–11** were synthesized via Stille coupling of compound **7** with compounds **8–9** in the presence of Pd(PPh₃)₄ catalyst, in a very good yield



Scheme 1. Synthesis of key molecule 10.

(≈82%). Furthermore, Knoevenagel condensation of compounds 10–11 with malononitrile in the presence of pyridine in refluxing chloroform affords target compounds; PQx (1) and TQx (2) in the good yields (≈75%). Similarly, Knoevenagel condensation of compounds; 10–11 with 2-cyanoacetic acid in the presence of piperidine in refluxing chloroform affords target molecules PQxD (3) and TQxD (4) in the good yields (≈70%). SAM molecules 1–4 were purified simply by recrystallization from methanol. The solubility of the new molecules 1–4 increases due to presence 4,4'-dimethoxytriphenylamine units and anchoring groups (CN/COOH or CN/CN). For example, compounds 2 and 4 are good soluble in common organic solvents, such as chlorobenzene, chloroform, and toluene. The chemical structures of 1–4 were confirmed by ^1H and ^{13}C NMR and mass spectrometry (See Supporting Information).

The optical, thermal, and electrochemical properties of SAM molecules 1–4 are displayed in **Table 1**. Newly synthesized molecules show good thermal stability with only ≈5% weight loss taking place at 328, 232, 248, and 218 °C for 1–4 respectively, obtained by thermogravimetric analysis (TGA) (Figure S1, Supporting Information). TGA analysis indicates compounds 1 and 3 with four rigid phenyl, and two TPA units exhibiting high thermal stability as compared to the compounds 2 and 4 with thiophene unit. The ultra-violet–visible (UV-vis) absorption spectrum of compounds TQx (2) and TQxD (4) in $o\text{-C}_6\text{H}_4\text{Cl}_2$ is significantly red-shifted ($\lambda_{\text{max}} = 374 \text{ nm}$, 360 nm ; **Figure 2a**) as compared to PQx (1) and PQxD (3) ($\lambda_{\text{max}} = 353 \text{ nm}$, 348 nm ; **Figure 2a**), reflecting that the presence of thiophene unit in molecules 2 and 4 is more effective in increasing conjugation as compared to the



Scheme 2. Synthetic routes to SAM molecules 1–4.

Table 1. Thermal, Optical, and Electrochemical Properties of Indicated Compounds.

| SAM | $T_d^a)$ [C] | λ_{abs} [soln] ^{b)} [nm] | $E_{ox}^c)$ [V] | HOMO ^{d)} [eV] | LUMO ^{e)} [eV] | ΔE_g [eV] ^{f)} |
|----------|-----------------|--|--------------------|----------------------------|----------------------------|------------------------------------|
| PQx [1] | 328 | 353 | 0.84 | -5.28 | -2.91 | 2.37 |
| TQx [2] | 232 | 374 | 0.84 | -5.28 | -3.03 | 2.25 |
| PQxD [3] | 248 | 348 | 0.84 | -5.28 | -2.87 | 2.41 |
| TQxD [4] | 218 | 360 | 0.86 | -5.30 | -2.97 | 2.33 |

^{a)}By TGA; ^{b)}UV-vis absorption spectra were recorded in *o*-C₆H₄Cl₂; ^{c)}By DPV in *o*-C₆H₄Cl₂ at 25 °C. All potentials reported with reference to Fc/Fc⁺ internal standard (at +0.64 V); ^{d)}Using HOMO = -(4.44 + 0.64 + E_{ox}) against NHE; ^{e)}Estimated from LUMO = HOMO + E_g ; ^{f)}Optical energy gap was calculated using 1240/ λ_{abs} (onset).

phenyl unit in molecules 1 and 3.^[53] The electrochemical properties of SAM molecules 1–4 were investigated by differential pulse voltammetry (DPV) in *o*-C₆H₄Cl₂ at 25 °C utilizing tetrabutylammonium hexafluorophosphate as the electrolyte^[55] (Figure 2b). The oxidation potentials of SAMs; 1–4 were calibrated employing ferrocene as an internal standard at +0.64 V. The HOMO energy levels of the SAM molecules 1–4 were calculated by the equation $E_{HOMO} = -(4.44 + 0.64 + E_{ox})$. The oxidation peaks of compounds 1–4 are located at +0.84 and +0.84 V, +0.84 V, and +0.86 V respectively, and the derived E_{HOMO} s of compounds 1–4 are thus estimated as -5.28 and -5.28 eV, -5.28 eV, -5.30 eV respectively. Furthermore, to ensure the first oxidation peak of compounds 1–4, measurements were carried out with/without added ferrocene during the DPV experiment (Figure S2, Supporting Information).

The thiophene/phenyl substituents of the conjugated backbones have no significant effect on the electrochemical properties, and thus E_{HOMO} levels of compounds 1–4 are almost identical. The optical bandgap of the compounds 1–4 is derived from the onset of the absorption spectra. The LUMO values are obtained by the addition of the HOMO and bandgap values (LUMO = HOMO + E_g). The estimated LUMO values are -2.91, -3.03, -2.87, and -2.97 eV for compounds 1–4 respectively.

To verify the intrinsic optical stability, a photoaging experiment under one sun illumination in air was conducted to assess the stability of SAMs; 1–4 in anhydrous *o*-dichlorobenzene solution (Figure S3, Supporting Information). The data indicate that there were no changes in the absorption spectra of 1–4 after 12 h of illumination. These results indicate that SAMs 1–4 exhibit good photostability.^[56] Furthermore, to access the electrochemical stability of the redox processes and oxidized species, we carried out cyclic voltammetry experiments for SAMs 1–4 (Figure S4, Supporting Information). The data demonstrate highly stable reversible oxidations, and that SAMs 1–4 show excellent electrochemical stability.^[56,57]

DFT calculations were employed to gain further insights into the electronic structures of compounds 1–4 at the B3LYP/6-31G* level of theory using the Gaussian 03 W program. The HOMOs of molecules 1–4 are primarily located on the triphenyl amine and phenyl units while the LUMOs are primarily located on quinoxaline backbone as well as thiophene/phenyl units attached to cyanoacrylic acid/dicyanovinylene groups. DFT-derived E_{HOMO} are -4.78, -4.78, -4.72, and -4.71 eV for 1–4, respectively, and the E_{LUMO} are -3.06, -3.17, -2.76, and -2.88 eV for 1–4, respectively. Note that the slight variation in

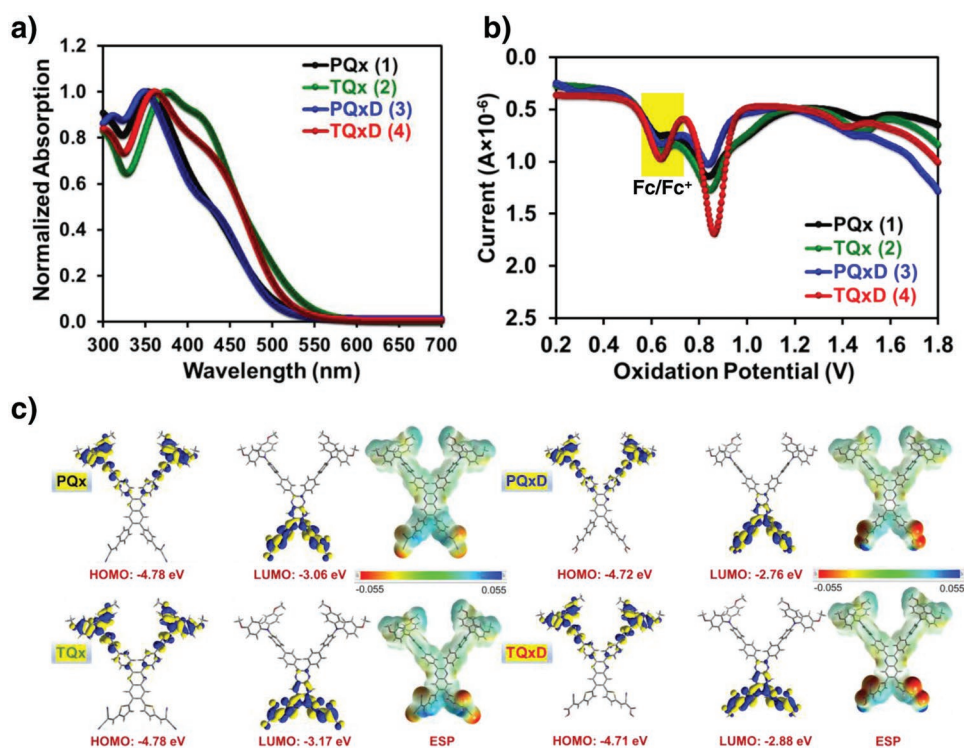


Figure 2. a) UV-vis absorption spectra of compounds 1–4 in *o*-C₆H₄Cl₂. b) DPV response curves of 1–4. c) DFT-derived energy levels and Electrostatic surface potential (ESP) mapping of 1–4.

the energy level trends found between DFT calculations and DPV measurements is not unexpected and likely originate from the different environmental conditions.^[58] Furthermore, we performed electrostatic potential (ESP) surface analysis of the PQx (1), TQx (2), PQxD (3) and TQxD (4) molecules to better understand the charge distribution on the molecules and evaluate possible sites that may interact with ITO surface (Figure 2c). On the top of these X-shaped molecules (Scheme 2; Figure 2c), they all have two triphenylamino side chain legs attached to the pyrazine unit of the quinoxaline moiety for donating electrons to the perovskite layer confirmed by the DFT calculations showing the electronic distributions of the HOMO levels (Figure 2c) localized in top legs for all SAM molecules. On the bottom of the X-shaped molecules (Scheme 2; Figure 2c), either phenyl (PQx and PQxD) or thiophene unit (TQx and TQxD) with the two-hand anchoring group (either -CN or/and -COOH) is attached to the thiophene/benzene unit of the quinoxaline moiety to interact with the ITO substrate via the cyano/carboxylic acid anchors to form SAM for TPSC. According to the DFT calculated results, the electrostatic potential (ESP) mapping images of the four SAM molecules (Figure 2c) reveal that high electron density (negative charges) mainly located on the electron-withdrawing end groups (cyano/carboxylic acid),^[53] providing a favorable condition for strong interaction between the end groups and the ITO surface to form self-assemble monolayer.^[59–62]

The XPS spectra of these four thin-film samples shown in Figure 3 have confirmed the attachment of these molecules on the ITO substrate with the spectral features of varied functional groups (C=C, C–N, and C–O), for which only –COOH feature occurs for the PQxD and TQxD samples. Then tin perovskite layer was deposited on these SAM substrates according

to a two-step method reported previously.^[31,33,35] Afterwards, C₆₀, BCP and silver layers were deposited on the perovskite layer step by step via thermal evaporation. Since our previous study^[35] indicates that the pre-heating of the ITO substrate affects the device performance quite significantly, we therefore first checked the device performance at varied pre-heating temperatures from 100 to 500 °C; the corresponding results are shown in Figure S5 (Supporting Information). For the TQx and TQxD devices, it shows the same trend for the device performance giving the best efficiencies at T = 100 °C. To understand this discrepancy, we measured the contact angles of SnI₂/DMSO on the TQx/ITO and TQxD/ITO substrates; the corresponding results are shown in Figure S6a,b (Supporting Information), respectively.

We did not observe big difference for the contact angles on different pre-heated substrates; for TQx/ITO, they are between 14.28° (400 °C) and 18.10° (100 °C); for TQxD/ITO, they are between 16.18° (400 °C) and 19.41° (100 °C). The pre-heating temperature at 100 °C seems to have largest contact angles among the others. However, these contact angles are relatively small, indicating the excellent hydrophilic property for this series of SAM.

Figure S7a,b (Supporting Information) show the cross-sectional SEM images for the perovskite produced on the TQx/ITO and TQxD/ITO substrates, respectively. It shows that the ITO preheated at 100 °C always generates thicker perovskite film than preheated at 400 °C. Furthermore, we also measured the GIWAXS images for the TQx/ITO and TQxD/ITO samples at incidence angle $\alpha = 0.02^\circ$, as the results shown in Figure S8a,b (Supporting Information), respectively. We found the evidence of π - π stacking for the SAM film at $q \approx 1.6 \text{ \AA}^{-1}$, which is more pronounced for preheating at 100 °C than at 400 °C. We also

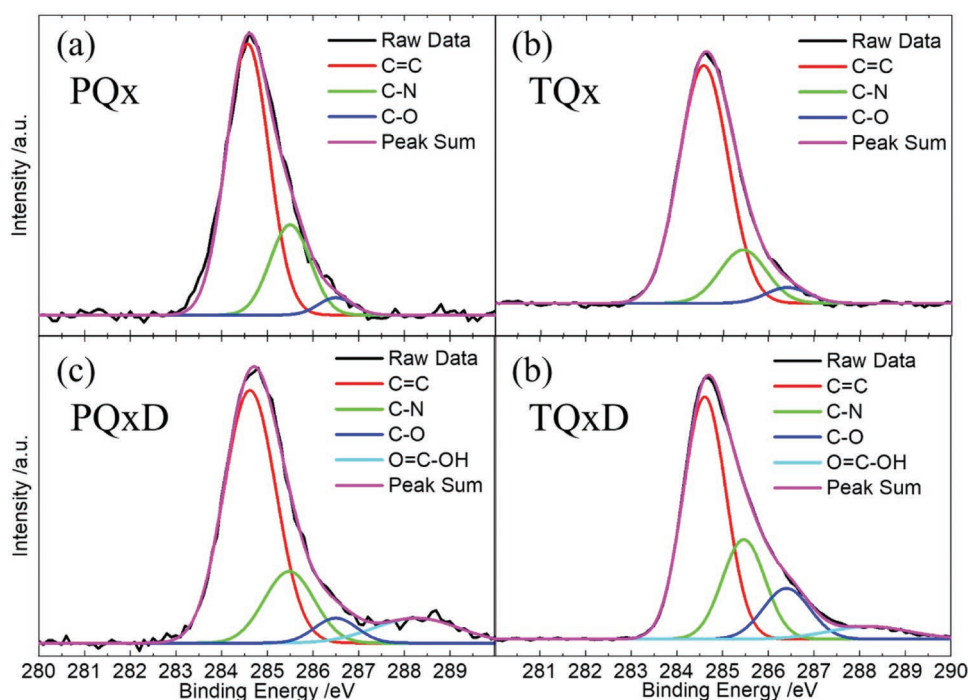


Figure 3. XPS spectra and corresponding deconvoluted components for a) PQx, b) TQx, c) PQxD, and d) TQxD.

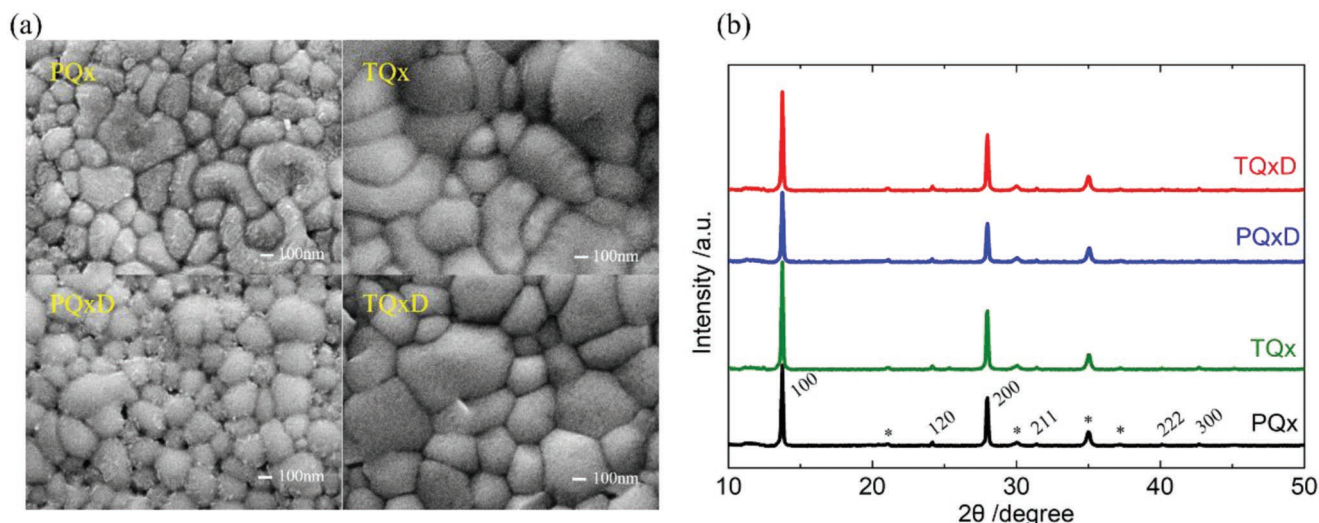


Figure 4. a) Top-view SEM images and b) XRD patterns for PQx, TQx, PQxD, and TQxD as indicated. The “*” symbol represents the diffraction patterns of ITO substrate.

carried out TCSPC measurements for tin perovskites deposited on TQx/ITO and TQxD/ITO substrates at varied preheating temperatures as the PL temporal profiles shown in Figure S9a,b (Supporting Information), respectively. The PL lifetimes exhibit an increasing trend from $T = 100\text{ }^{\circ}\text{C}$ to $T = 500\text{ }^{\circ}\text{C}$ for both cases, indicating that the tin perovskite fabricated at the preheating temperature $100\text{ }^{\circ}\text{C}$ has the greatest charge transfer rate than all the others. Therefore, the ITO preheating temperature was setting at $100\text{ }^{\circ}\text{C}$ for all studies reported hereafter.

Figure 4a,b shown the top-view SEM images and XRD patterns of the perovskite nanocrystals fabricated using the four SAM substrates, respectively. It is apparent that the film morphology and crystallinity are superior for the thiophene-based SAM (TQx and TQxD) than for the benzene-based SAM (PQx and PQxD). **Figure 5** shows the AFM profiles for the perovskites produced on these four substrates. It indicates that the average film roughness is 44 nm for PQx and 36 nm for PQxD, but the roughness significantly decreases to 14 nm for both TQx

and TQxD samples. Therefore, the functional group thiophene has the ability to produce uniform and close-packed perovskite film with greater crystallinity than the SAMs with the benzene substitute.

For the optical properties, **Figure 6a** shows the UV-vis absorption and PL spectra for the four films, all have similar bandgaps and PL peak positions. **Figure 6b** shows the TCSPC results with the PL temporal profiles fitted by a bi-exponential decay function; the corresponding fitted parameters are summarized in Table S1 (Supporting Information). It shows that the TQ series samples have smaller average PL lifetimes than the PQ series samples, consistent with the film morphology and crystallinity to be better for the former than for the later.

Figure 7a shows the energy level diagram for all the components used to fabricate a TPSC. The VB and CB levels of the SAM samples were determined from the UPS spectra (Figure S10, Supporting Information) and tauc plots of the absorption spectra (Figure S11, Supporting Information). All

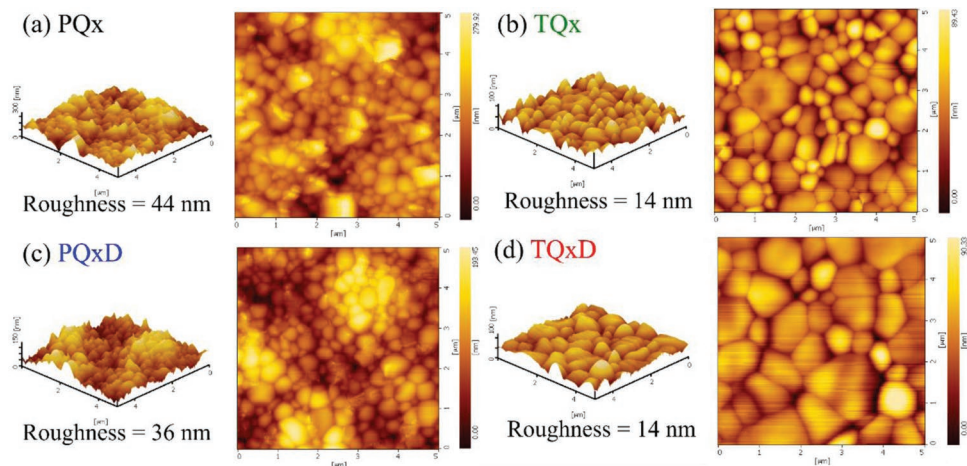


Figure 5. AFM images and their 3D profiles for a) PQx, b) TQx, c) PQxD, and d) TQxD.

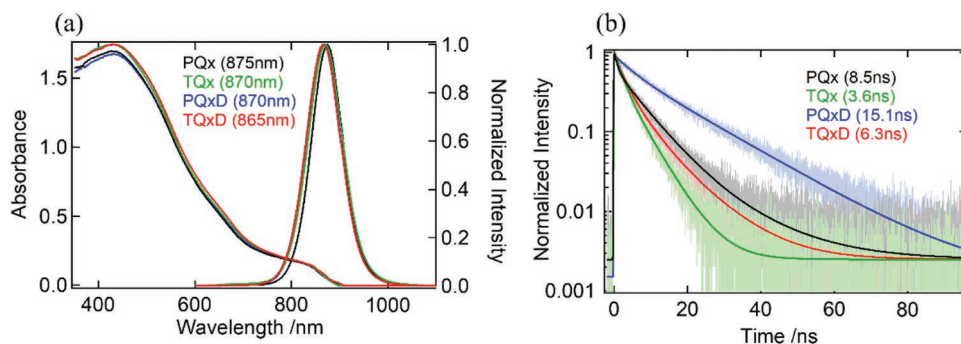


Figure 6. a) UV-vis and PL spectra and b) TCSPC PL decay profiles for PQx, TQx, PQxD, and TQxD thin-film samples, respectively.

the energy levels of SAM match well with tin perovskite so that holes are feasible to transfer from the VB of perovskite to the HOMO of SAM while electrons are feasible to transfer from CB of perovskite to LUMO of C₆₀. The TPSC devices were fabricated according to the structure ITO/SAM/perovskite/C60/BCP/Ag as shown in Figure 7a. Figure 7b shows the *J*-*V* curves of the four SAM devices with the trend TQxD (8.3%) > TQx (8.0%) > PQxD (7.1%) > PQx (6.1%); the corresponding photovoltaic parameters are shown in Table 2 for comparison. Figure 7c shows the IPCE spectra for these four devices, with the integrated current density matching with those of the *J*-*V* scans (Figure 7b). Total 40 devices were fabricated for each SAM (Table S2–S5, Supporting Information), and cor-

responding boxplots of performance are shown in Figure S12 (Supporting Information). Figure S13a–d (Supporting Information) shows typical forward and reverse *J*-*V* scans for PQx, TQx, PQxD, and TQxD, respectively, for which negligible effect of hysteresis was observed for all devices. Figure 7d shows the enduring stability of the four devices in glovebox in dark condition. It is remarkable to note that the PQxD and TQxD devices retained the efficiencies over 90% of its original efficiency for over 1600 h.

To understand why the TQx and TQxD devices outperform the PQx and PQxD devices, we performed electrochemical impedance spectral (EIS) measurements for these four devices under four bias voltages, 0.2, 0.3, 0.4, and 0.5 V

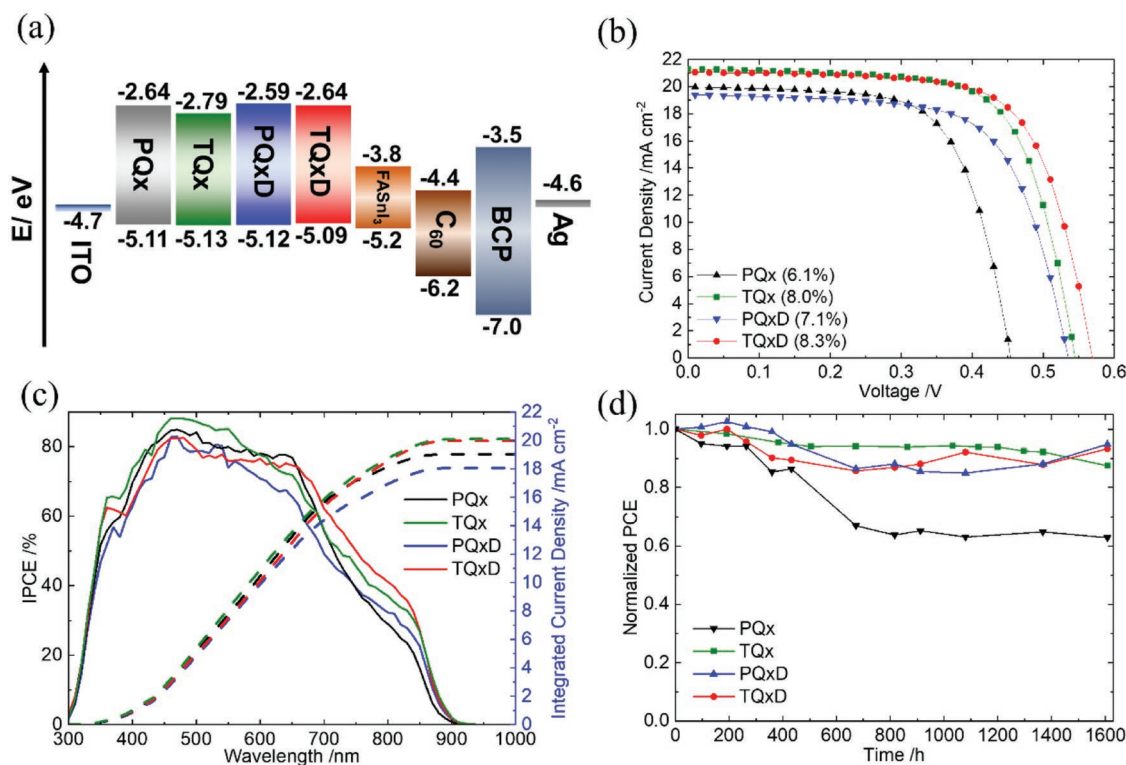


Figure 7. a) Energy-level diagram for each SAM species measured by UPS spectra and Tauc plots, b) *J*-*V* curves for the devices made of PQx, TQx, PQxD, and TQxD, c) corresponding IPCE spectra and integrated current-density and d) enduring performance stability for all devices stored in a glovebox.

Table 2. Photovoltaic Parameters Obtained from the Statistic of J - V Curves.

| SAM | V_{oc} /V | J_{sc} /mA cm ⁻² | FF /% | PCE /% |
|------|-------------|-------------------------------|----------|-----------|
| PQx | 0.465±0.054 | 17.46±3.24 | 65.8±5.0 | 5.32±0.68 |
| * | 0.455 | 19.97 | 66.6 | 6.1 |
| TQx | 0.519±0.079 | 20.33±2.65 | 67.4±4.4 | 7.10±0.96 |
| * | 0.546 | 21.30 | 69.0 | 8.0 |
| PQxD | 0.499±0.053 | 18.22±2.70 | 66.4±4.9 | 6.01±0.89 |
| * | 0.542 | 19.28 | 68.1 | 7.1 |
| TQxD | 0.550±0.064 | 19.42±2.78 | 68.5±3.7 | 7.30±1.08 |
| * | 0.574 | 21.05 | 68.8 | 8.3 |

*Best performance

in dark. The Nyquist plots of the four devices are shown in Figure S14 (Supporting Information) with all plots showing one semicircle feature; they were fitted with only one RC circuit with the resistance corresponding to the charge recombination process.

Figure 8a shows the semilogarithmic plots of charge recombination resistance versus bias voltage, and it exhibits the trend with $TQxD \approx TQx > PQxD > PQx$ consistent with the performance trend shown in Figure 7b. In addition, we also perform the space-charge-limited current (SCLC) measurements for the four SAM films in order to estimate the charge mobility for each SAM. According to the Mott–Gurney law, the SCLC plots shown in Figure 8b give the hole mobility with the order $TQx > TQxD > PQxD > PQx$, which is consistent with the trends of EIS and the device performance. Therefore, the superior performance of TQxD and TQx is due to their retarded charge recombination and enhanced hole mobility as we have observed in both experiments. We therefore conclude that both cyano group and carboxylic acid are good linkers to

form SAM on the ITO substrate, but the thiophene unit has better performance than the benzene unit due to the better charge transport and retarded charge recombination for the former than for the later.

3. Conclusions

Four X-shaped quinoxaline-based molecules, PQx, TQx, PQxD, and TQxD, were designed and synthesized as SAM for tin-based perovskite solar cells. Cyano/cyano or cyano/carboxylic acid groups are conjugated with phenyl ring (PQx and PQxD) or thiophene unit (TQx and TQxD) to attach in the benzene side of the quinoxaline moiety to serve as the two-hand anchoring group to bond on the ITO surface, while the two-leg triphenylamino groups were attached in the pyrazine side of quinoxaline via a benzene linker to effectively donate electrons to the perovskite layer, both were confirmed by the DFT calculations. We found that both CN/CN and CN/COOH are good anchoring groups for the four organic molecules to form SAM on the ITO surface, and the thiophene unit in TQx and TQxD plays a key role to form smooth and uniform tin perovskite nanocrystals with excellent morphology, crystallinity, and film roughness. The SAM devices exhibit the performance with the order of PCE showing $TQxD$ (8.3%) > TQx (8.0%) > $PQxD$ (7.1%) > PQx (6.1%), which is consistent with the trends of the corresponding hole mobility (SCLC), retarded charge recombination (EIS) and hole transfer rate (TCSPC). Note that the device made of TQxD as SAM (8.3%) outperforms the device made of carbazole-based SAM (6.5%) previously reported^[35] and the TQxD device is so far the best SAM-based device for TPSC. All devices except PQx showed great enduring stability for the performance retaining $\approx 90\%$ of their original values for shelf storage over 1600 h. This study thus gives a guidance for designing more advanced SAM molecules applied for tin-based perovskite solar cells.

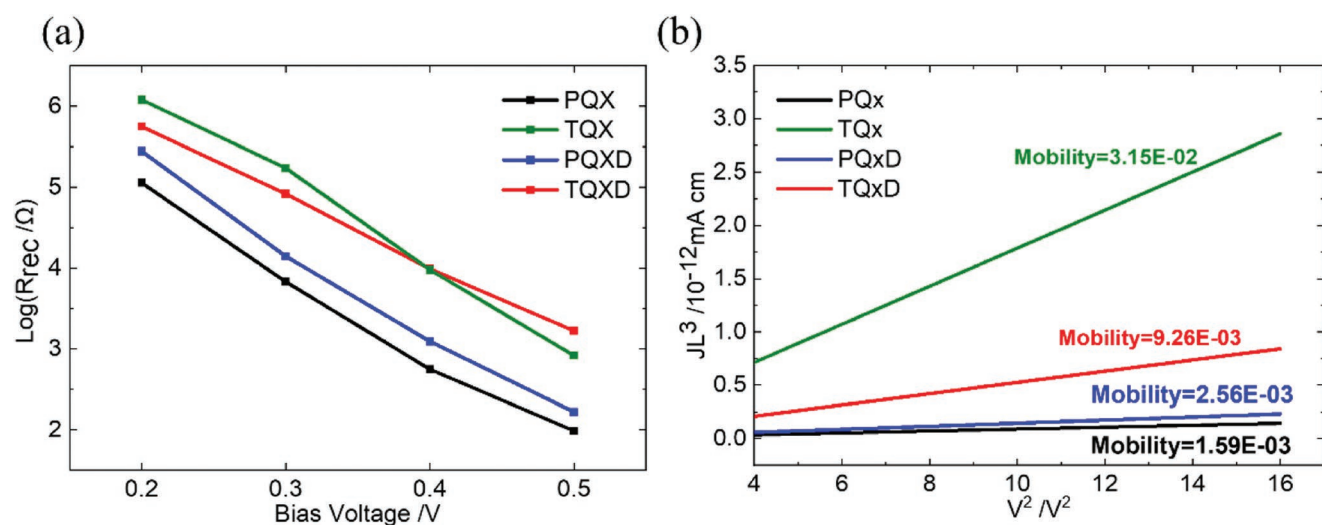


Figure 8. a) Semilogarithmic plots for charge recombination resistance (R_{rec}) versus bias voltage in dark condition and b) Space-charge limited current (SCLC) plots showing the hole mobilities (in unit of $\text{cm}^2 \text{V}^{-1} \text{s}^{-1}$) for PQx, TQx, PQxD, and TQxD.

Supporting Information

Supporting Information is available from the Wiley Online Library or from the author.

Acknowledgements

S.N.A. and C.-H.K. contributed equally to this work. The authors thank Prof. C. S. Lin and Ms. Y.T. Lee of Instrumentation Center, National Taiwan University for FEG-SEM experiments. M.-C. Chen gratefully acknowledges the funding provided by the Ministry of Science and Technology of Taiwan (MOST 111-2113-M-008-004-MY3), National Science and Technology Council in Taiwan (NSTC 111-2622-8-008-006) and NCU-Covestro Research Center. E. W. Diau thanks the support by National Science and Technology Council (NSTC), Taiwan (grant No. NSTC 111-2634-F-A49-007, NSTC 111-2123-M-A49-001) and the Center for Emergent Functional Matter Science of National Yang Ming Chiao Tung University (NYCU) from The Featured Areas Research Center Program within the framework of the Higher Education Sprout Project by the Ministry of Education (MOE) in Taiwan.

Conflict of Interest

The authors declare no conflict of interest.

Data Availability Statement

Research data are not shared.

Keywords

quinoxaline, self-assembled monolayers, tin perovskite solar cells

Received: November 29, 2022

Revised: January 11, 2023

Published online:

- [1] Z. Guo, A. K. Jena, G. M. Kim, T. Miyasaka, *Energy Environ. Sci.* **2022**, *15*, 3171.
- [2] S. N. Afraj, A. Velusamy, C.-Y. Chen, J.-S. Ni, Y. Ezhumalai, C.-H. Pan, K.-Y. Chen, S.-L. Yau, C.-L. Liu, C.-H. Chiang, C.-G. Wu, M.-C. Chen, *J. Mater. Chem. A* **2022**, *10*, 11254.
- [3] S. N. Afraj, D. Zheng, A. Velusamy, W. Ke, S. Cuthriell, X. Zhang, Y. Chen, C. Lin, J.-S. Ni, M. R. Wasielewski, W. Huang, J. Yu, C.-H. Pan, R. D. Schaller, M.-C. Chen, M. G. Kanatzidis, A. Facchetti, T. J. Marks, *ACS Energy Lett.* **2022**, *7*, 2118.
- [4] T.-W. Chen, S. N. Afraj, S.-H. Hong, L.-H. Chou, A. Velusamy, C.-Y. Chen, Y. Ezhumalai, S.-H. Yang, I. Osaka, X.-F. Wang, M.-C. Chen, C.-L. Liu, *ACS Appl. Energy Mater.* **2022**, *5*, 4149.
- [5] E. W.-G. Diau, *A. C. S. Energy Lett.* **2017**, *2*, 334.
- [6] E. W.-G. Diau, E. Jokar, M. Rameez, *ACS Energy Lett.* **2019**, *4*, 1930.
- [7] X. Chen, Z. Jia, Z. Chen, T. Jiang, L. Bai, F. Tao, J. Chen, X. Chen, T. Liu, X. Xu, C. Yang, W. Shen, W. E. I. Sha, H. Zhu, Y. Yang, *Joule* **2020**, *4*, 1594.
- [8] W. Ma, T. Jiang, Z. Yang, H. Zhang, Y. Su, Z. Chen, X. Chen, Y. Ma, W. Zhu, X. Yu, H. Zhu, J. Qiu, X. Liu, X. Xu, Y. Yang, *Adv. Sci.* **2021**, *8*, 2003728.
- [9] W. Ma, Y. Su, Q. Zhang, C. Deng, L. Pasquali, W. Zhu, Y. Tian, P. Ran, Z. Chen, G. Yang, G. Liang, T. Liu, H. Zhu, P. Huang, H. Zhong, K. Wang, S. Peng, J. Xia, H. Liu, X. Liu, Y. M. Yang, *Nat. Mater.* **2022**, *21*, 210.
- [10] A. Velusamy, S. N. Afraj, S. Yau, C.-L. Liu, Y. Ezhumalai, P. Kumaresan, M.-C. Chen, *J. Chin. Chem. Soc.* **2022**, *69*, 1253.
- [11] S. Vegiraju, W. Ke, P. Priyanka, J.-S. Ni, Y.-C. Wu, I. Spanopoulos, S. L. Yau, T. J. Marks, M.-C. Chen, M. G. Kanatzidis, *Adv. Funct. Mater.* **2019**, *29*, 1905393.
- [12] W. Ke, P. Priyanka, S. Vegiraju, C. C. Stoumpos, I. Spanopoulos, C. M. M. Soe, T. J. Marks, M.-C. Chen, M. G. Kanatzidis, *J. Am. Chem. Soc.* **2018**, *140*, 388.
- [13] C.-C. Lin, S. N. Afraj, A. Velusamy, P.-C. Yu, C.-H. Cho, J. Chen, Y.-H. Li, G.-H. Lee, S.-H. Tung, C.-L. Liu, M.-C. Chen, A. Facchetti, *ACS Nano* **2021**, *15*, 727.
- [14] W. Ke, M. G. Kanatzidis, *Nat. Commun.* **2019**, *10*, 965.
- [15] B.-B. Yu, Z. Chen, Y. Zhu, Y. Wang, B. Han, G. Chen, X. Zhang, Z. Du, Z. He, *Adv. Mater.* **2021**, *33*, 2102055.
- [16] N. Sun, W. Gao, H. Dong, Y. Liu, X. Liu, Z. Wu, L. Song, C. Ran, Y. Chen, *ACS Energy Lett.* **2021**, *6*, 2863.
- [17] E. Jokar, H.-S. Chuang, C.-H. Kuan, H.-P. Wu, C.-H. Hou, J.-J. Shyue, E. Wei-Guang Diau, *J. Phys. Chem. Lett.* **2021**, *12*, 10106.
- [18] X. Jiang, F. Wang, Q. Wei, H. Li, Y. Shang, W. Zhou, C. Wang, P. Cheng, Q. Chen, L. Chen, Z. Ning, *Nat. Commun.* **2020**, *11*, 1245.
- [19] X. Jiang, Z. Zang, Y. Zhou, H. Li, Q. Wei, Z. Ning, *Acc. Mater. Res.* **2021**, *2*, 210.
- [20] E. Jokar, P.-Y. Cheng, C.-Y. Lin, S. Narra, S. Shahbazi, E. Wei-Guang Diau, *ACS Energy Lett.* **2021**, *6*, 485.
- [21] E. Jokar, P. H. Hou, S. S. Bhosale, H. S. Chuang, S. Narra, E. Wei-Guang Diau, *Chem. Sus. Chem.* **2021**, *14*, 4415.
- [22] E. Jokar, Z. Y. Huang, S. Narra, C.-Y. Wang, V. Kattoor, C.-C. Chung, E. W.-G. Diau, *Adv. Energy Mater.* **2018**, *8*, 1701640.
- [23] C.-M. Tsai, Y.-P. Lin, M. K. Pola, S. Narra, E. Jokar, Y.-W. Yang, E. W.-G. Diau, *ACS Energy Lett.* **2018**, *3*, 2077.
- [24] S. Narra, C.-Y. Lin, A. Seetharaman, E. Jokar, E. W.-G. Diau, *J. Phys. Chem. Lett.* **2021**, *12*, 12292.
- [25] X. Jiang, H. Li, Q. Zhou, Q. Wei, M. Wei, L. Jiang, Z. Wang, Z. Peng, F. Wang, Z. Zang, K. Xu, Y. Hou, S. Teale, W. Zhou, R. Si, X. Gao, E. H. Sargent, Z. Ning, *J. Am. Chem. Soc.* **2021**, *143*, 10970.
- [26] E. Jokar, C.-H. Chien, A. Fathi, M. Rameez, Y.-H. Chang, E. W.-G. Diau, *Energy Environ. Sci.* **2018**, *11*, 2353.
- [27] E. Jokar, C.-H. Chien, C.-M. Tsai, A. Fathi, E. W.-G. Diau, *Adv. Mater.* **2019**, *31*, 1804835.
- [28] Z. Zhu, X. Jiang, D. Yu, N. Yu, Z. Ning, Q. Mi, *ACS Energy Lett.* **2022**, *7*, 2079.
- [29] X. Liu, K. Yan, D. Tan, X. Liang, H. Zhang, W. Huang, *ACS Energy Lett.* **2018**, *3*, 2701.
- [30] W. Han, G. Ren, J. Liu, Z. Li, H. Bao, C. Liu, W. Guo, *ACS Appl. Mater. Interfaces* **2020**, *12*, 49297.
- [31] C.-H. Kuan, G.-S. Luo, S. Narra, S. Maity, H. Hiramatsu, Y.-W. Tsai, J.-M. Lin, C.-H. Hou, J.-J. Shyue, E. Wei-Guang Diau, *Chem. Eng. J.* **2022**, *450*, 138037.
- [32] X. Liu, T. Wu, X. Luo, H. Wang, M. Furue, T. Bessho, Y. Zhang, J. Nakazaki, H. Segawa, L. Han, *ACS Energy Lett.* **2022**, *7*, 425.
- [33] S. Shahbazi, M.-Y. Li, A. Fathi, E. W.-G. Diau, *ACS Energy Lett.* **2020**, *5*, 2508.
- [34] R. Shang, Z. Zhou, H. Nishioka, H. Halim, S. Furukawa, I. Takei, N. Ninomiya, E. Nakamura, *J. Am. Chem. Soc.* **2018**, *140*, 5018.
- [35] D. Song, S. Narra, M.-Y. Li, J.-S. Lin, E. W.-G. Diau, *ACS Energy Lett.* **2021**, *6*, 4179.
- [36] A. Al-Ashouri, A. Magomedov, M. Roß, M. Jošt, M. Talaikis, G. Chistiakova, T. Bertram, J. A. Márquez, E. Köhnen, E. Kasparavičius, S. Levenco, L. Gil-Escrig, C. J. Hages, R. Schlatmann, B. Rech, T. Malinauskas, T. Unold, C. A. Kaufmann,

- L. Korte, G. Niaura, V. Getautis, S. Albrecht, *Energy Environ. Sci.* **2019**, *12*, 3356.
- [37] G. Kapil, T. Bessho, Y. Sanehira, S. R. Sahamir, M. Chen, A. K. Baranwal, D. Liu, Y. Sono, D. Hirotsu, D. Nomura, K. Nishimura, M. A. Kamarudin, Q. Shen, H. Segawa, S. Hayase, *ACS Energy Lett.* **2022**, *7*, 966.
- [38] E. Aktas, N. Phung, H. Köbler, D. A. González, M. Méndez, I. Kafedjiska, S.-H. Turren-Cruz, R. Wenisch, I. Lauermaun, A. Abate, E. Palomares, *Energy Environ. Sci.* **2021**, *14*, 3976.
- [39] F. Ali, C. Roldán-Carmona, M. Sohail, M. K. Nazeeruddin, *Adv. Energy Mater.* **2020**, *10*, 2002989.
- [40] Y. Bai, Q. Dong, Y. Shao, Y. Deng, Q. Wang, L. Shen, D. Wang, W. Wei, J. Huang, *Nat. Commun.* **2016**, *7*, 12806.
- [41] Ç. Kirbiyık, K. Kara, D. A. Kara, M. Z. Yiğit, B. İstanbullu, M. Can, N. S. Sarıciğci, M. Scharber, M. Kuş, *Appl. Surf. Sci.* **2017**, *423*, 521.
- [42] A. Ullah, K. H. Park, H. D. Nguyen, Y. Siddique, S. F. A. Shah, H. Tran, S. Park, S. I. Lee, K.-K. Lee, C.-H. Han, K. Kim, S. Ahn, I. Jeong, Y. S. Park, S. Hong, *Adv. Energy Mater.* **2022**, *12*, 2103175.
- [43] E. Yalcin, M. Can, C. Rodriguez-Seco, E. Aktas, R. Pudi, W. Cambarau, S. Demic, E. Palomares, *Energy Environ. Sci.* **2019**, *12*, 230.
- [44] S. Y. Kim, S. J. Cho, S. E. Byeon, X. He, H. J. Yoon, *Adv. Energy Mater.* **2020**, *10*, 2002606.
- [45] A. Mishra, M. K. R. Fischer, P. Bäuerle, *Angew. Chem., Int. Ed.* **2009**, *48*, 2474.
- [46] T. Wu, Y. Wang, Z. Dai, D. Cui, T. Wang, X. Meng, E. Bi, X. Yang, L. Han, *Adv. Mater.* **2019**, *31*, 1900605.
- [47] L. Li, Y. Wu, E. Li, C. Shen, H. Zhang, X. Xu, G. Wu, M. Cai, W.-H. Zhu, *Chem. Commun.* **2019**, *55*, 13239.
- [48] Y. Wang, Q. Liao, J. Chen, W. Huang, X. Zhuang, Y. Tang, B. Li, X. Yao, X. Feng, X. Zhang, M. Su, Z. He, T. J. Marks, A. Facchetti, X. Guo, *J. Am. Chem. Soc.* **2020**, *142*, 16632.
- [49] H. Zhang, Y. Wu, W. Zhang, E. Li, C. Shen, H. Jiang, H. Tian, W.-H. Zhu, *Chem. Sci.* **2018**, *9*, 5919.
- [50] Y. Liao, K. Pan, L. Wang, Q. Pan, W. Zhou, X. Miao, B. Jiang, C. Tian, G. Tian, G. Wang, H. Fu, *ACS Appl. Mater. Interfaces* **2013**, *5*, 3663.
- [51] D. Heredia, J. Natera, M. Gervaldó, L. Otero, F. Fungo, C.-Y. Lin, K.-T. Wong, *Org. Lett.* **2010**, *12*, 12.
- [52] C.-Y. Lo, D. Kumar, S.-H. Chou, C.-H. Chen, C.-H. Tsai, S.-H. Liu, P.-T. Chou, K.-T. Wong, *ACS Appl. Mater. Interfaces* **2016**, *8*, 27832.
- [53] M. Guo, C.-Y. Lin, S.-J. Liou, Y. J. Chang, Y. Li, J. Li, M. Wei, *J. Mater. Chem. A* **2021**, *9*, 25086.
- [54] N. Zhou, K. Prabakaran, B. Lee, S. H. Chang, B. Harutyunyan, P. Guo, M. R. Butler, A. Timalina, M. J. Bedzyk, M. A. Ratner, S. Vegiraju, S. Yau, C.-G. Wu, R. P. H. Chang, A. Facchetti, M.-C. Chen, T. J. Marks, *J. Am. Chem. Soc.* **2015**, *137*, 4414.
- [55] S. Vegiraju, G.-Y. He, C. Kim, P. Priyanka, Y.-J. Chiu, C.-W. Liu, C.-Y. Huang, J.-S. Ni, Y.-W. Wu, Z. Chen, G.-H. Lee, S.-H. Tung, C.-L. Liu, M.-C. Chen, A. Facchetti, *Adv. Funct. Mater.* **2017**, *27*, 1606761.
- [56] S. Zhang, R. Wu, C. Mu, Y. Wang, L. Han, Y. Wu, W.-H. Zhu, *ACS Mater. Lett.* **2022**, *4*, 1976.
- [57] S. N. Afraj, C.-C. Lin, A. Velusamy, C.-H. Cho, H.-Y. Liu, J. Chen, G.-H. Lee, J.-C. Fu, J.-S. Ni, S.-H. Tung, S. Yau, C.-L. Liu, M.-C. Chen, A. Facchetti, *Adv. Funct. Mater.* **2022**, *32*, 2200880.
- [58] Y.-D. Lin, K.-M. Lee, S. H. Chang, T.-Y. Tsai, H.-C. Chung, C.-C. Chou, H.-Y. Chen, T. J. Chow, S.-S. Sun, *ACS Appl. Energy Mater.* **2021**, *4*, 4719.
- [59] T. Wu, Y. Wang, X. Li, Y. Wu, X. Meng, D. Cui, X. Yang, L. Han, *Adv. Energy Mater.* **2019**, *9*, 1803766.
- [60] L. Zhang, J. M. Cole, *ACS Appl. Mater. Interfaces* **2015**, *7*, 3427.
- [61] W.-C. Chen, S. Nachimuthu, J.-C. Jiang, *Sci. Rep.* **2017**, *7*, 4979.
- [62] Y. Ooyama, S. Inoue, T. Nagano, K. Kushimoto, J. Ohshita, I. Imae, K. Komaguchi, Y. Harima, *Angew. Chem., Int. Ed.* **2011**, *50*, 7429.